Electronic Supplementary Information for

Crystal Phase-Dependent Electrocatalytic Hydrogen Evolution Performance of Ruthenium-Boron Intermetallics

Xu Zou,‡ Lina Wang,‡ Xuan Ai, Hui Chen, and Xiaoxin Zou*

State Key Laboratory of Inorganic Synthesis and Preparative Chemistry, College of Chemistry, Jilin University, Changchun 130012, P. R. China;

‡ X. Zou and L. Wang contributed equally to this work.

* E-mail: xxzou@jlu.edu.cn

1. Theoretical Section

1.1. Computation Details.

The calculations for all the materials were carried out by the *Vienna ab initio simulation package* (VASP)[1-2] based on the density functional theory (DFT). Perdew-Burke-Ernzerhof (PBE)[3] exchange-correlation functional within the generalized gradient approximation (GGA) was used for the structural relaxations and electronic structure calculations. The cutoff energy of plane-wave set[4] is 400 eV. While the convergence thresholds of atomic force and total energy were set as 0.02 eV/Å and 10^{-4} eV, respectively. The appropriate Monkhorst-Pack *k*-point meshes 7×7×7, 11×11×7, 5×5×5, 9×9×9, 11×11×3, 9×9×9, 11×11×9 and 11×11×4 were chosen for the bulk calculations of Pt, Ru, Ru_7B_3, RuB, Ru_2B_3, RuB_2-I, RuB_2-II and RuB_2-III. In regard to the slab models of surfaces, 5×5×1 *k*-point mesh was employed for all of them[5]. The symmetrization was switched off and the dipolar correction was included for all the calculations of slab models. The DFT-D2 method[6] was used to correct the *van der Waals* interaction. The crystal orbital Hamiltonian population (COHP) was obtained by LOBSTER code[7-10].

For the slab models, we constructed 1×1 supercell for Ru_7B_3 and 2×2 supercells for other ruthenium-boron intermetallics by cleaving the bulk structure with metal-termination along the (001) direction, where a vacuum layer of 15 Å between slabs was added to avoid inter-layer interactions. The thickness of Ru (0001) and Pt (111) slab models were four atomic layers and the others were eight atomic layers. During the slab calculations, we relaxed the upper half of atom layers and the remaining were kept frozen.

1.2. Computations of Formation Energy for Ruthenium-Boron Intermetallics.

The formation energy was calculated by the equation: $\Delta H_f = [E_{total}(Ru_xB_y) - xE_{total}(Ru) - yE_{total}(B)]/(x+y)$, where $E_{total}(Ru_xB_y)$ is the total energy for one formula unit of the compound, $E_{total}(Ru)$ and $E_{total}(B)$ are the energies of pure metal Ru and α-B at the ground state, and x and y are the number of Ru and B atoms, respectively.

1.3. Computations of Free-Energy for the Hydrogen Evolution Reaction.

The Gibbs free-energy (ΔG_{H^*}) of H^* adsorption was obtained by the equation $\Delta G_{H^*} = \Delta E_{H^*} + \Delta ZPE - T\Delta S$, where ΔE_{H^*}, ΔZPE and ΔS are the adsorption energy, zero point energy and entropy change[11]. ΔE_{H^*} is defined as $\Delta E_{H^*} = E(\text{surface} + \text{nH}) - E[\text{surface} + (\text{n-1})\text{H}] - 1/2\ E(H_2)$, where $E(\text{surface} + \text{nH})$, $E[\text{surface} + (\text{n-1})\text{H}]$ and $E(H_2)$ are energies of n, n-1 hydrogen atom adsorbed on the surface, and a gas phase H_2 molecule. ΔZPE was calculated by using the equation $\Delta ZPE = ZPE(H^*) - 1/2ZPE(H_2)$, $T\Delta S$ was obtained by using the equation $T\Delta S \approx -1/2\ TS(H_2)$. Since $TS(H_2)$ is 0.41eV for H_2 at 298K and 1atm, $T\Delta S \approx -0.205$ eV.

2. Experimental Section

2.1. Chemicals and Reagents.

Potassium aquapentachlororuthenate(III) (K_2RuCl_5) and platinum tetrachloride ($PtCl_4$, 99.9%) were purchased from Aladdin Chemistry Co., Ltd. Magnesium boride (**MgB_2**) was purchased from Alfa Aesar Chemicals Co., Ltd. Magnesium powder (Mg) was purchased from Shantou Xilong Chemical Factory.

Sulfuric acid (H_2SO_4), potassium hydroxide (KOH) and isopropanol were purchased from Beijing Chemical Factory. Platinum on graphitized carbon (20 wt% Pt/C) and Nafion® perfluorinated resin solution were purchased from Sigma-Aldrich. Highly purified water (> 18 MΩ cm resistivity) was obtained from a PALL PURELAB Plus system.

2.2. Synthesis of Ruthenium-Boron Intermetallics.

Four ruthenium-boron intermetallics with different crystal phases by solid phase synthesis. First, a certain amount of potassium aquapentachlororuthenate(III) (K_2RuCl_5), magnesium diboride (MgB_2) and magnesium powder (Mg) were ground and then loaded into a quartz tube, which was then sealed in a vacuum atmosphere (1.0 Pa). The exceptions are the synthesis of Ru_2B_3 and RuB_2, which does not require to add Mg. To avoid the effects of moisture, weighting all chemicals were under infrared light. Next, put the quartz tube into the tubular furnace for heating with a speed of 2 ^oC/min. The heating temperature was 700-950 ^oC, maintaining some time in the temperature (generally 3-10 hours). After cooling to room temperature, the product was immersed in 0.5 M H_2SO_4 solution for 3 hours to remove unreacted reactants (*i.e.*, Mg powder) and by-product (*i.e.*, $MgCl_2$). Finally, the sample was washed three times with distilled water and ethanol, respectively, and then dried at 80 ^oC. The detailed synthesis parameters were shown in Table S3. RuB_2 was synthesized according to our previously-reported procedure[12].

2.3. Synthesis of Ru nanoparticles:

K_2RuCl_5 (51.9 mg, 0.25 mmol) and Mg (14.6 mg, 0.6 mmol) were ground and loaded into a quartz tube, which was then sealed in a vacuum atmosphere (1.0 Pa). The quartz tube was heated in a tubular furnace for 4 h at 700 °C, and the heating rate was 2 °C/min. After cooling, the sample was immersed in 0.5 M H_2SO_4 solution for 3 hours. Finally, the sample was washed three times with distilled water and ethanol, respectively, and then dried at 80 ^oC.

2.4. Synthesis of Pt nanoparticles:

$PtCl_4$ (84.2 mg, 0.25 mmol) and Mg (24.3 mg, 1.0 mmol) were ground and loaded into a quartz tube, which was then sealed in a vacuum atmosphere (1.0 Pa). The quartz tube was heated in a tubular furnace for 4 h at 500 °C, and the heating rate was 2 °C/min. After cooling, the sample was immersed in 0.5 M H_2SO_4 solution for 3 hours. Finally, the sample was washed three times with distilled water and ethanol, respectively, and then dried at 80 ^oC.

2.5. Characterizations.

Powder X-ray diffraction (PXRD) of ruthenium-boron intermetallics were recorded on a Rigaku D/Max 2550 X-ray diffractometer. The range of diffraction angle was 10-80^o, and the scan speed was 8 ^{o}/min. The transmission electron microscope (TEM) images were achieved with a Philips-FEI Tecnai G2STwin microscope equipped with a field emission gun operating at 200 kV. The specific surface area of ruthenium-boron intermetallics were obtained useing the Brunauer-Emmett-Teller (BET) method on a Micromeritics ASAP 2020 M system.

2.6. Electrochemical Measurements.

The electrochemical measurements were researched with a three-electrode system using a CH Instrument (Model 660E). Saturated calomel electrode (SCE) and Hg/HgO electrode were used as

reference electrodes in acid (0.5 M H_2SO_4 solution) and alkaline (1.0 M KOH solution) systems, respectively. Carbon rod was used as the counter electrode. To prepare the working electrode: (1) 8 mg of sample was dispersed into 400 μL of isopropanol and 400 μL of conductive polymer binder (0.3% Nafion solution); (2) 2 μL of this solution was dropped onto a glassy carbon electrode (GCE) with a diameter of 3mm and dried in the air; (3) 2 μL of conductive polymer binder was dropped on top and dried to be used as working electrode. The loading mass is 0.281 mg cm^{-2}. During the test, N_2 was continuously introduced into the electrochemical cell. Linear sweep voltammetry (LSV) measurements were used with the scan rate of 0.5 mV/s and 85% *iR*-correction. We used chronopotentiometric measurements to evaluate the stability of the material at current density of 10 mA cm^{-2} without *iR*-correction. Convert the potential to the potential *versus* the reversible hydrogen electrode (RHE) according to formula (1) in acid condition and formula (2) in alkaline condition:

$$E_{vs\ RHE} = E_{vs\ SCE} + E^{o}_{SCE} + 0.059pH \qquad (1)$$

$$E_{vs\ RHE} = E_{vs\ Hg/HgO} + E^{o}_{\ Hg/HgO} + 0.059pH \qquad (2)$$

Reference electrodes were calibrated according to the method reported by Boetter and co-workers[13]. For comparison, the catalytic activities of Ru, Pt and commercial 20 wt.% Pt/C were evaluated under the same test conditions and loading.

The j_{BET} value was normalized with the Brunauer-Emmett-Teller (BET) surface area from formula (3):

$$j_{BET} = \frac{i \times 100}{S \times m_{loading} \times A_{(BET)}} \qquad (3)$$

where i is the current obtained with 85% *iR*- correction; S is the geometric area of GCE (0.071 cm^2); $m_{loading}$ is the loading mass of sample on the GCE (0.281 mg cm^{-2}); $A_{(BET)}$ is the BET surface area (m^2/g).

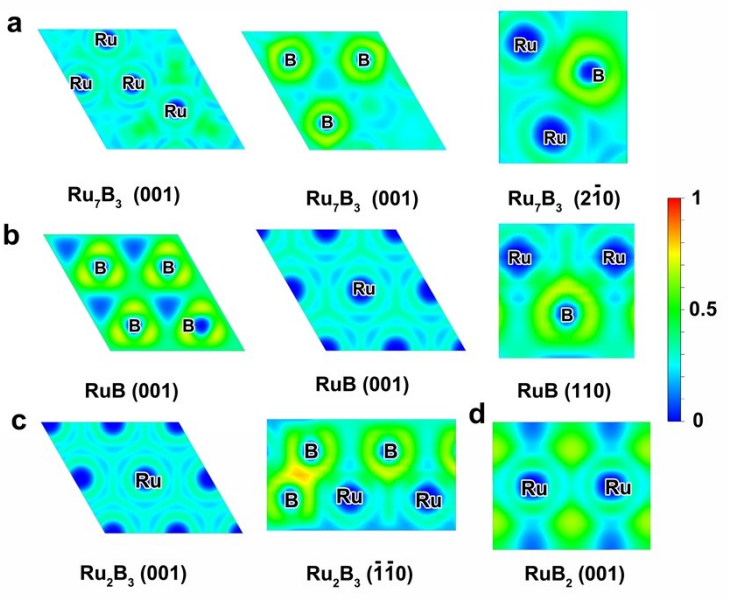

Fig. S1. Electron location function (ELF) of different planes for (a) Ru_7B_3, (b) RuB, (c) Ru_2B_3, (d) RuB_2.

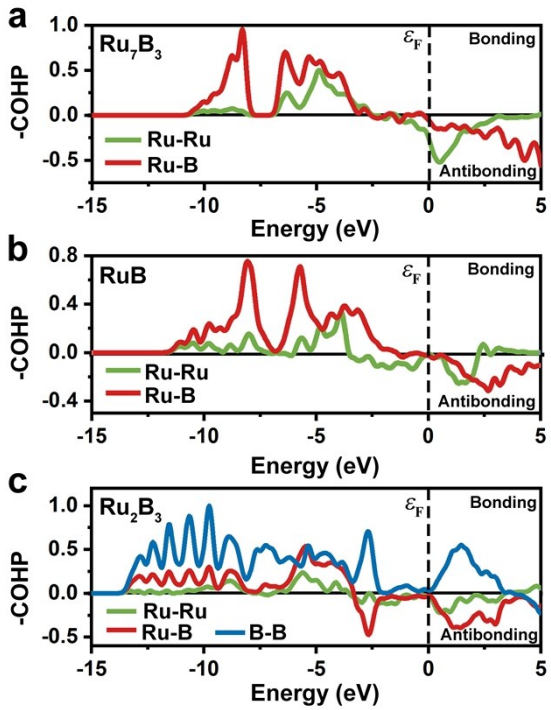

Fig. S2. Crystal Orbital Hamilton Populations (COHP) curves of (a)Ru_7B_3, (b) RuB, (c) Ru_2B_3.

Table S1. The integrated COHP (-ICOHP) of Ru_7B_3, Ru_2B_3, RuB and RuB_2 for different interactions.

	Ru-B (eV)	B-B(eV)	Ru *d*-B *sp*(eV)
Ru_7B_3	2.85	--	1.93
RuB	2.80	--	1.95
Ru_2B_3	2.37	5.05	1.75
RuB_2	2.21	5.31	1.64

Table S2. The formation energy of different ruthenium-boron intermetallics.

	Formation energy (eV/atom)
Ru_7B_3	-0.138
RuB	-0.331
Ru_2B_3	-0.332
RuB_2	-0.286

Table S3. The experimental parameters for the synthesis of ruthenium-boron intermetallics.

Sample Name	K_2RuCl_5	MgB_2	Mg	Temperature and Time
Ru_7B_3	0.2 mmol	0.13 mmol	0.123 mmol	950 ^oC, 5 h
RuB	0.15mmol	0.1 mmol	0.15mmol	800 ^oC, 9 h
Ru_2B_3	0.15 mmol	0.5 mmol	--	700 ^oC, 5 h
RuB_2	0.167mmol	0.5 mmol	--	950 ^oC, 3 h

Table S4. The BET surface areas of different ruthenium-boron intermetallics.

	BET Surface Area (m^2/g)
Ru_7B_3	1.4
RuB	3.6
Ru_2B_3	12.3
RuB_2	12.5

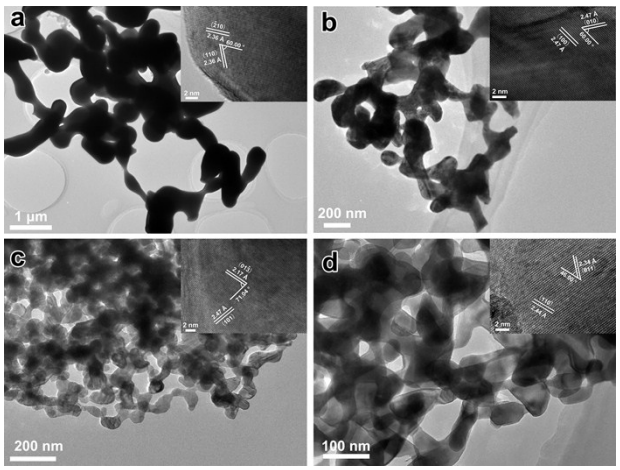

Fig. S3. TEM and HR-TEM (inset) images of four ruthenium-boron intermetallics (a) Ru_7B_3, (b) RuB, (c) Ru_2B_3, (d) RuB_2

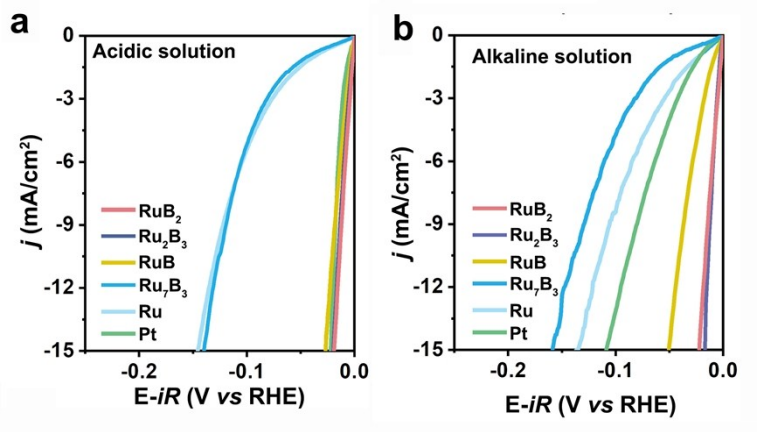

Fig. S4. Polarization curves of Ru_7B_3, RuB, Ru_2B_3, RuB_2, metallic Ru and Pt for the HER with 85% *iR*-compensation. (a) 0.5 M H_2SO_4 solution. (b) 1 M KOH solution.

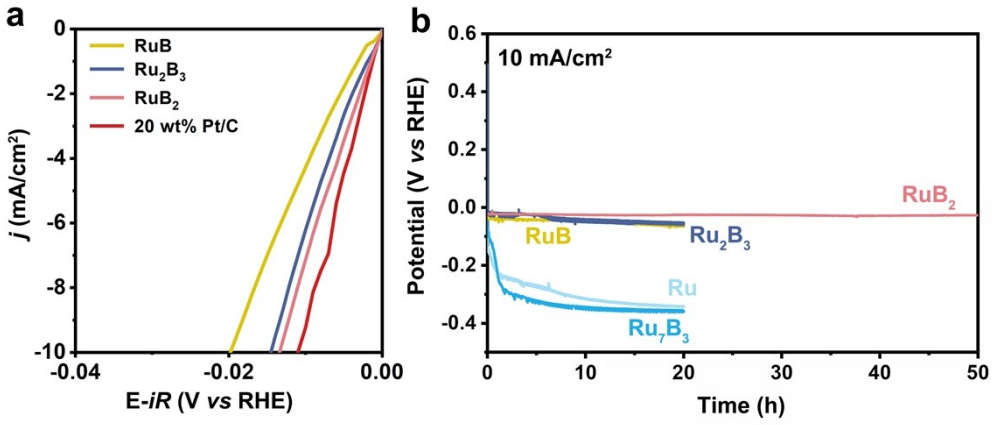

Fig. S5. (a) Polarization curves of RuB, Ru_2B_3, RuB_2 and commercial 20 wt% Pt/C for HER in 0.5 M H_2SO_4 solution with 85% *iR*-compensation. (b) Chronopotentiometric curve of Ru_7B_3, RuB, Ru_2B_3, RuB_2 and metallic Ru in 0.5 M H_2SO_4 solution at 10 mA/cm_{goe}^2.

Table S5. Tafel slop of different ruthenium-boron intermetallics.

	0.5 M H_2SO_4 (mV/dec)	1.0 M KOH (mV/dec)
Ru_7B_3	71.9	73.3
RuB	32.7	30.6
Ru_2B_3	30.3	27.3
RuB_2	30.2	27.9
Pt	26.1	52.5
Ru	61.6	73.3

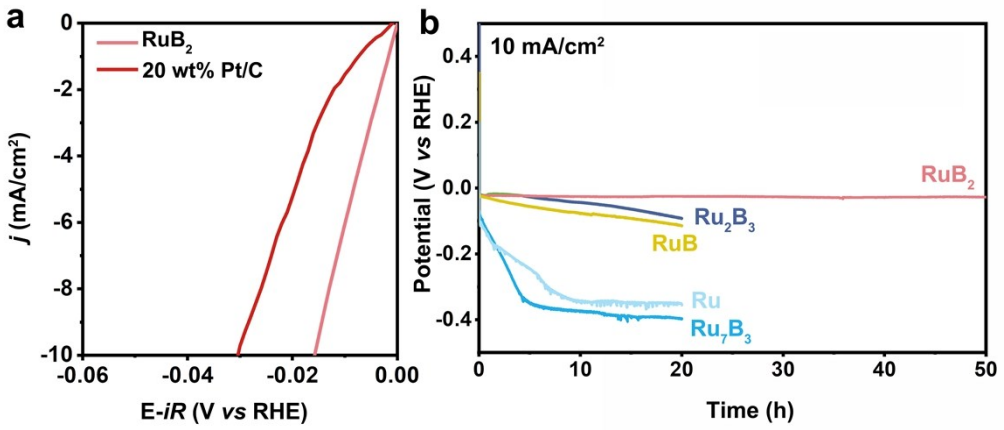

Fig. S6. (a) Polarization curves of RuB_2 and commercial 20 wt% Pt/C for the HER in 1.0 M KOH solution with 85% *iR*-compensation. (b) Chronopotentiometric curve of Ru_7B_3, RuB, Ru_2B_3, RuB_2 and metallic Ru in 1.0 M KOH solution at 10 mA/cm_{goe}^2.

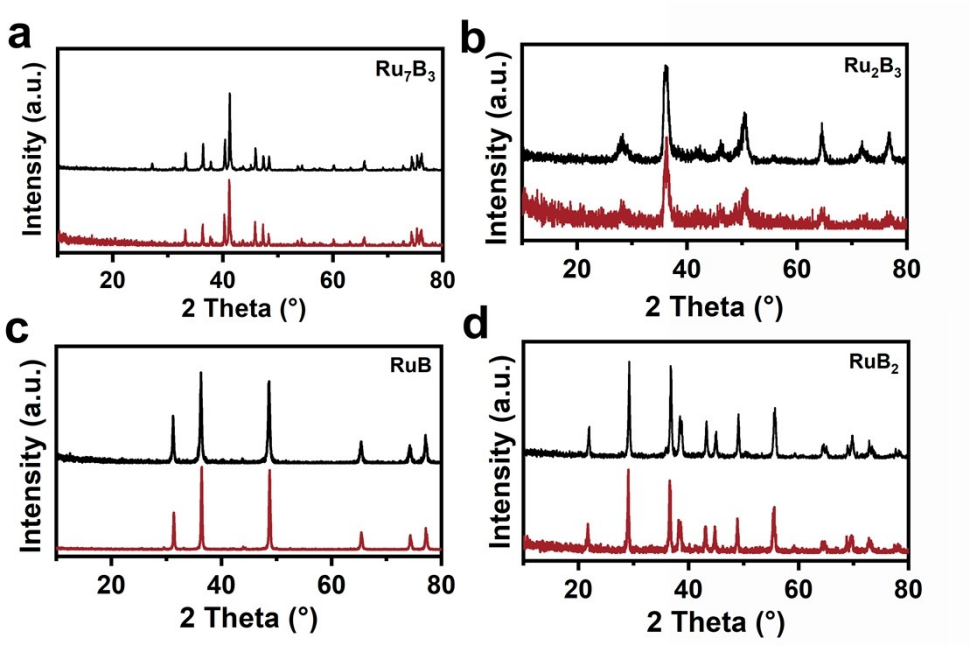

Fig. S7. The XRD patterns of the four ruthenium-boron intermetallics. Black line is before catalysis, red line is after 10 h chronopotentiometric test. (a)Ru_7B_3. (b)Ru_2B_3. (c)RuB. (d)RuB_2.

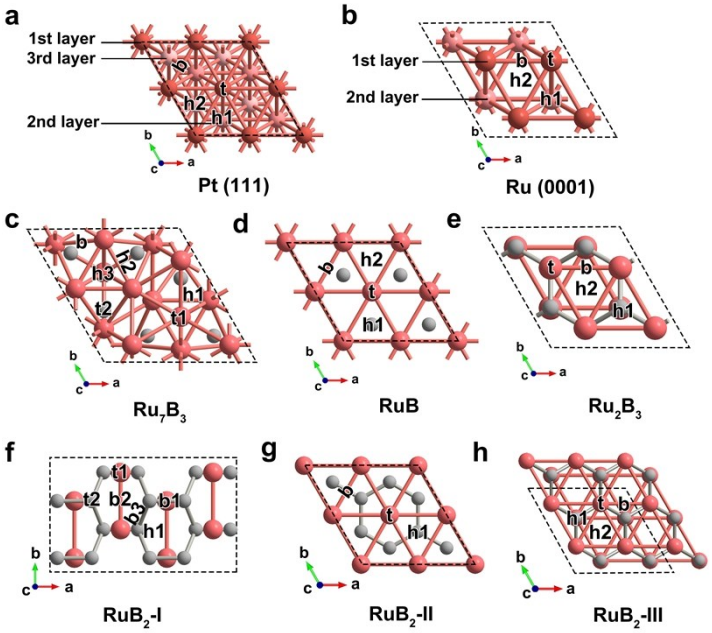

Fig. S8. The adsorption H* sites for (a) Pt (111) (b) Ru (0001) (c) Ru_7B_3 (001) (d) RuB (001) (e) Ru_2B_3 (001) (f) RuB_2-I (001) (g) RuB_2-II (001) and (h) RuB_2-III (001) surfaces with metal-termination.

Table S6. The ΔE_{H^*} of RuB_2-I at different sites. The t, b and h denote the Top, Bridge and Hollow sites, respectively. The bolded values are ΔE_{H^*} in the most stable adsorption sites.

	t1 (eV)	**t2 (eV)**	**b1 (eV)**	**b2 (eV)**	**b3 (eV)**	**h1 (eV)**
RuB_2-I	-0.06	Unstable	-0.32	**-0.34**	Unstable	-0.16

Table S7. The ΔE_{H^*} of RuB_2-II and RuB_2-III at different sites. The bolded values are ΔE_{H^*} in the most stable adsorption sites.

	Top(eV)	**Bridge(eV)**	**h1(eV)**	**h2(eV)**
RuB_2-II	Unstable	Unstable	**-1.91**	/
RuB_2-III	-0.61	Unstable	-0.80	**-1.00**

Table S8. The ΔE_{H^*} of Ru_7B_3 at different sites. The t, b and h denote the Top, Bridge and Hollow sites, respectively. The bolded values are ΔE_{H^*} in the most stable adsorption sites.

	t1(eV)	**t2(eV)**	**b(eV)**	**h1(eV)**	**h2(eV)**	**h3(eV)**
Ru_7B_3	-0.63	-0.27	**-0.64**	-0.63	0.01	0.08

Table S9. The ΔE_{H^*} of Pt (111), Ru (0001), RuB and Ru_2B_3 at different sites. The bolded values are ΔE_{H^*} in the most stable adsorption sites. Ru_2B_3 (Ⅰ) and (Ⅱ) are Ru layers bond to isolated boron atoms and puckered boron layers, respectively.

	Top(eV)	**Bridge(eV)**	**h1(eV)**	**h2(eV)**
RuB	-0.26	Unstable	-0.48	**-0.59**
Ru_2B_3 (Ⅰ)	-0.26	Unstable	-0.35	**-0.49**
Ru_2B_3 (Ⅱ)	-0.57	Unstable	-0.71	**-0.88**
Pt (111)	**-0.57**	-0.52	-0.49	-0.54
Ru (0001)	-0.24	Unstable	-0.65	**-0.68**

Table S10. The ΔG_{H^*} of the most stable adsorption sites for different materials. The bold values are ΔG_{H^*} obtained at 100 % H* coverage on the most stable adsorption sites. Ru_2B_3 (Ⅰ) and (Ⅱ) are Ru layers bond to isolated boron atoms and puckered boron layers, respectively.

	ΔG_{H^*}/eV
Ru_7B_3	-0.42
RuB	**-0.23**
Ru_2B_3 (Ⅰ)	**-0.17**
Ru_2B_3 (Ⅱ)	**-0.17**
RuB_2-I	**-0.04**
RuB_2-II	-1.71
RuB_2-III	-0.79
Pt (111)	**-0.10**
Ru (0001)	**-0.38**

Table S11. The integrated COHP (-ICOHP) of Ru-H for different RuB_2.

	-ICOHP (eV)	Adsorption site	-ICOHP/unit cell (eV)
RuB_2- Ⅰ	1.72	bridge	3.44
RuB_2-II	1.44	3-fold hollow	4.32
RuB_2-III	1.40	3-fold hollow	4.20

Supplementary References

1. G. Kresse and J. Furthmüller, *Comput. Mater. Sci.*, 1996, **6**, 15.
2. G. Kresse and J. Furthmüller, *Phys. Rev. B*, 1996, **54**, 11169.
3. J. P. Perdew, K. Burke and M. Ernzerhof, *Phys. Rev. Lett.*, 1996, **77**, 3865.
4. P. E. Blöchl, *Phys. Rev. B*, 1994, **50**, 17953.
5. H. J. Monkhorst and J. D. Pack, *Phys. Rev. B*, 1976, **13**, 5188.
6. S. J. Grimme, *Comp. Chem.*, 2006, **27**, 1787.
7. R. Dronskowski and P. E. Blöchl, *J. Phys. Chem.*, 1993, **97**, 8617.
8. V. L. Deringer, A. L. Tchougreeff and R. Dronskowski, *J. Phys. Chem. A*, 2011, **115**, 5461.
9. S. Maintz, V. L. Deringer, A. L. Tchougreeff and R. Dronskowski, *J. Comput. Chem.*, 2013, **34**, 2557.
10. S. Maintz, V. L. Deringer, A. L. Tchougreeff and R. Dronskowski, *J. Comput. Chem.*, 2016, **37**, 1030.
11. J. K. Nørskov, T. Bligaard, A. Logadottir, J. R. Kitchin, J. Chen, S. Pandelov and U. Stimming, *J. Electrochem. Soc.*, 2005, **152**, 23.
12. Q. Li, X. Zou, X. Ai, H. Chen, L. Sun and X. Zou, *Adv. Energy Mater.*, 2018, 1803369.
13. M. S. Burke, M. G. Kast, L. Trotochaud, A. M. Smith and S. W. Boettcher, *J. Am. Chem. Soc.*, 2015, **137**, 3638.